Published in final edited form as:
Biosens Bioelectron. 2014 April 15; 54: 610–616. doi:10.1016/j.bios.2013.11.059.

Stretchable Electrochemical Impedance Sensors for Intravascular Detection of Lipid-Rich Lesions in New Zealand White Rabbits

Hung Cao[*,1,3], **Fei Yu**[*,1], **Yu Zhao**[*,2], **Nick Scianmarello**[2], **Juhyun Lee**[1,3], **Wangde Dai**[4], **Nelson Jen**[1,3], **Tyler Beebe**[1,3], **Rongsong Li**[1,3], **Ramin Ebrahimi**[3], **Donald S. Chang**[3], **Freny V. Mody**[3], **John Pacella**[5], **Yu-Chong Tai**[2], and **Tzung Hsiai**[1,3]

[1]Department of Biomedical Engineering, University of Southern California, Los Angeles, CA Los Angeles, CA

[2]Department of Electrical Engineering, California Institute of Technology, Pasadena, CA

[3]Division of Cardiology, Department of Medicine, School of Medicine, University of California

[4]The Heart Institute of Good Samaritan Hospital, Los Angeles, CA

[5]Division of Cardiology, School of Medicine, University of Pittsburgh, Pittsburgh, PA

Abstract

Flexible electronics have enabled catheter-based intravascular sensing. However, real-time interrogation of unstable plaque remains an unmet clinical challenge. Here, we demonstrate the feasibility of stretchable electrochemical impedance spectroscopy (EIS) sensors for endoluminal investigations in New Zealand White (NZW) rabbits on diet-induced hyperlipidemia. A parylene C (PAC)-based EIS sensor mounted on the surface of an inflatable silicone balloon affixed to the tip of an interrogating catheter was deployed 1) on the explants of NZW rabbit aorta for detection of lipid-rich atherosclerotic lesions, and 2) on live animals for demonstration of balloon inflation and EIS measurements. An input peak-to-peak AC voltage of 10 mV and sweeping-frequency from 300 kHz to 100 Hz were delivered to the endoluminal sites. Balloon inflation allowed EIS sensors to be in contact with endoluminal surface. In the oxidized low-density-lipoprotein (oxLDL)-rich lesions from explants of fat-fed rabbits, impedance magnitude increased significantly by 1.5-fold across the entire frequency band, and phase shifted ~5 degrees at frequencies below 10 kHz. In the lesion-free sites of the normal diet-fed rabbits, impedance magnitude increased by 1.2-fold and phase shifted ~5 degrees at frequencies above 30 kHz. Thus, we demonstrate the feasibility of stretchable intravascular EIS sensors for identification of lipid rich lesions, with a translational implication for detecting unstable lesions.

Corresponding author: Tzung K. Hsiai, MD, PhD, Department of Medicine (Cardiology), Bioengineering, and Physiology, David Geffen School of Medicine, Henry Samueli School of Engineering and Applied Science, University of California Los Angeles, Los Angeles, CA 90073, THsiai@mednet.ucla.edu.
*The authors contributed equally.

Keywords

Stretchable micro-sensor; electrochemical impedance spectroscopy; balloon inflation; atherosclerotic lesions; New Zealand White rabbits

1. Introduction

Atherosclerosis is a systemic disease associated with focal and eccentric lesions (Fung, 1997). Atherosclerotic plaques usually contain high levels of inflammatory activity, due to oxidized lipids and foam cells (Bamford et al., 1991). The rupture of individual plaques is the primary underlying mechanism for myocardial infarction and stroke (Bamford, Sandercock, Dennis, Burn, & Warlow, 1991). Nevertheless, real-time detection of rupture-prone or unstable atherosclerotic lesions remains an unmet clinical challenge.

The advent of stretchable electronics provide intimal sensing of biomechanical and biophysical signals from tissues or organ systems otherwise difficult with conventional technologies (D.-H. Kim et al., 2011). Recently, our laboratory has developed micro-electromechanical systems (MEMS)-based thermal sensors for real-time interrogation of atherogenic fluid shear stress in the setting of oxidized low-density lipoprotein (oxLDL) and/or lipid-laden macrophages (Ai et al., 2008; Hamilton et al., 2008). We further demonstrated that spatial ($\partial\tau/\partial x$) and temporal ($\partial\tau/\partial t$) variations in shear stress regulate post-translational modifications of LDL; namely, oxidation and nitration, as well as recruitment of monocytes (Ai et al., 2008; Hsiai et al., 2007; Hwang, Michael, et al., 2003; Hwang, Saha, et al., 2003). These findings led to our novel observation that oxLDL and macrophages changed the electrochemical properties in the vessel wall that can be measured by electrochemical impedance spectroscopy (EIS) (Konings, Mali, & Viergever, 1997; Streitner et al., 2009; Suselbeck et al., 2005).

It is well recognized that tissue has a capacitive characteristic and its frequency-dependent electric impedance (Z) varies with its on-site composition and structure. In explants of the atherosclerotic lesions in the human aortic arch, we have reported increases in frequency-dependent electrochemical impedance magnitude by nearly 1.5-fold compared to the lesion-free sites (F. Yu, Ai, Dai, Yu, & Hsiai, 2011). Thus, real-time intravascular detection of the impedance changes in oxLDL-rich lesions holds promise to assess unstable plaque.

Electrochemical impedance spectroscopy (EIS) has been employed for detecting frequency-dependent changes in tissue impedance. A group of German investigators recently reported the application of a linear 4-point microelectrode that was affixed to a 2 centimeters long balloon catheter in NZW rabbits (Konings et al., 1997; Streitner et al., 2009; Suselbeck et al., 2005). Unlike the lengthy 4-point microelectrodes, the advantage of our bipolar microelectrode sensor lies in its concentric configuration (300 μm in diameter) that is conformal to the non-homogeneous tissue composition, non-planar endoluminal surface, and non-uniform electric current distribution of the atherosclerosis. Distinct from the large surface area (4-point) designed by the German group, our concentric bipolar microelectrode sensor provides a 2,000-fold reduction in dimension that can be conjugated with other catheter-based sensors such as ultrasonic transducers.

Concentric bipolar microelectrode sensors measure the non-Faradaic tissue impedance as a result of non-homogeneities of oxLDL and/or foam cell infiltrates in the atherosclerotic lesions (Virmani, Kolodgie, Burke, Farb, & Schwartz, 2000). Using equivalent circuits to simulate frequency-dependent changes in vessel impedance magnitude and phase, we have established specific electric elements in the working and counter electrode interfaces (F. Yu, Ai, et al., 2011; Fei Yu et al., 2012). When an alternating voltage (AC) is applied to the lesion site, the current can be detected and frequency-dependent electric impedance (Z) can be calculated. Z is the summation of a real number (r) and the resistance (X_c) multiplied by the imaginary number (i), defined as $Z = r + X_c i$ (Aroom et al., 2009). By recording the endoluminal Z across a sweeping-frequency range, the specific frequency-dependent electrical and dielectric properties can be determined (Foster & Schwan, 1996).

In this context, we deployed flexible and stretchable concentric bipolar microelectrode sensors in New Zealand White (NZW) rabbits. In response to balloon inflation, the concentric sensor detected an increase in endoluminal impedance magnitude in the oxLDL-rich lesions from explants of fat-fed rabbit aortas. The balloon-inflatable sensors were further applied for *in vivo* demonstration of EIS measurements in real time. The impedance magnitude increased upon a minimal contact with the endolumen after balloon inflation in the normal-fed rabbits. Hence, our findings demonstrated the potential clinical utility of stretchable EIS sensors to assess lipid-rich atherosclerotic lesions with an implication for identifying unstable plaque in humans.

2. Designs and Methods

a) Implementation of the flexible and stretchable concentric bipolar EIS with balloon

The manufacturing process required 4 main steps: **1**) fabricating the silicone balloon (Fig. 1B-a-a), **2**) assembling the sealed tubing connecting the balloon to a syringe, **3**) micro-fabricating the impedance sensor (Fig. 1B-b), and **4**) securing the impedance sensor to the balloon (Fig. 1B-c). First, steel tubing with an outer diameter (OD) of 0.008 inches (200 μm) (McMaster-Carr, Santa Fe Springs, CA) was immersed into AZ9260 photoresist (PR) (AZ Electronic Materials, Branchburg, NJ); followed by a baking process for 10 minutes at 100°C. A second coating was then applied and baked for 10 minutes to form the inner layer of the balloon. Nusil 6820 silicone (Nusil Technology LLC, Carpinteria, CA) was used for its low Young's modulus - 4.4 MPa and high elongation - 175%). The silicone was thoroughly mixed in a 1:1 ratio of part A and part B, and then painted onto the surface of PR and the capillary tubing. An opening was intentionally created for the subsequent PR release (Fig. 1B-a-ii). Ensuring an even coverage of the balloon is important for symmetrical inflation. The modulus of elasticity increased with prolonged curing duration and temperature. Afterwards, the balloon was fully submerged into a beaker of acetone to dissolve the PR; thereby, forming the cavity and allowing for the removal of the inner steel tube. The hole on the top was sealed with further silicone painting. The balloon was set over a parylene-coated silicon wafer and baked for 10 minutes at 100 °C. PAC facilitated peeling the balloon, and having rested it on a wafer created a planar surface for securing the impedance sensor.

In parallel, a 30 gauge Luer-lok needle was epoxied into a 5 cm section of similar capillary tubing. The free end of the tubing was then epoxied over a 30 cm section of 200 μm steel tubing. The steel tubing was more flexible and less brittle than the capillary tubing, rendering a more robust device for intravascular interrogation. This assembly was cured in an oven at 100°C, checked for blockage by pushing air into a beaker of water via a syringe, and then dried in an oven. The open end was inserted into that of the balloon's capillary tubing and secured into place. Epoxy was spread over the silicone in contact with the capillary tubing to prevent balloon delamination (Fig. 1B-c).

To fabricate the impedance sensor, we deposited a 5-μm-thick bottom PAC onto a hexamethyldisilazane-treated (HMDS) silicon wafer. Then a metal layer of gold (Au) (0.2 μm) was deposited by thermal evaporation and patterned by chemical wet etching. After the deposition of another 5-μm-thick PAC layer, the impedance sensing electrodes and connecting pads were selectively exposed by oxygen plasma etching. The overall device outlines were finally defined by etching through the PAC layer. The device was then peeled off from silicon substrate.

To assemble the impedance sensor to the balloon, we applied epoxy to the flat side of the balloon with the sensor openings facing up. Next, the two connecting pads were connected to a coaxial wire using conductive epoxy, and then fully encapsulated and fixed onto the tubing by epoxy. The sinusoidal lines connecting the sensing electrodes and the pads allowed the sensor to stretch in response to balloon inflation (Fig. 1A and 1B).

b) Real-time intravascular acquisition

In compliance with the Institutional Animal Care and Use Committee (IACUC) at the University of Southern California, four male New Zealand White (NZW) rabbits (10-week-old: mean body weight ~ 2 kg) were purchased from a local breeder (Irish Farms, Norco, CA). NZW rabbits are established as a model of atherosclerotic biology with plaques accessible to catheter interrogation. Two animals were fed a high-fat, high cholesterol diet (Newco® 1.5% cholesterol & 6% peanut oil). After 8 weeks, explants of aortas were interrogated for intravascular electrochemical impedance spectroscope (EIS). Another two animals were used for feasibility of *in vivo* EIS measurements.

The rabbits were anesthetized for percutaneous access. Intravascular ultrasound (IVUS) probe and concentric bipolar microelectrodes were sterilized by Electron Beam technology (Titans SureBeam™) and heparinized to prevent thrombosis. A femoral cut-down were performed and a 2-French (distal O.D.) Tracker-10, 80/15 guide catheter (Target Therapeutic) were inserted under binocular magnification and heparin administered (150 units/kg). The catheter and a Dasher-14 Steerable Guide wire (Target Therapeutic) were then advanced under fluoroscopic guidance (Phillips BV-22HQ C-arm) into the aortic arch (Ai et al., 2009). The catheter and guide wire were withdrawn to the thoracic aorta, and lastly, abdominal aorta for similar interrogations. Four or more replicates were performed at each site. AC signals with peak-to-peak voltages of 10 mV and frequencies ranging from 100 Hz to 300 kHz were delivered to the sites. The magnitudes and phases of the impedances were acquired at 20 data points per frequency decade.

c) Immunohistochemistry

A portion of each aorta was fixed in 4% paraformaldehyde, embedded in paraffin and serially sectioned at 5 μm for histological analyses. Foam cells were identified by Sudan black stain, lipids with oil-red-O (Holvoet et al., 2001; Holvoet, Vanhaecke, Janssens, Van de Werf, & Collen, 1998; Verhamme et al., 2002), macrophages with anti-CD68 antibody, and oxLDL with mAb4E6 (Holvoet et al., 1998) as previously published (F. Yu, Ai, et al., 2011; Fei Yu et al., 2012).

d) Statistical Analysis

The data on lesion sizes and electrochemical impedance were analyzed by Student's t-test for comparison between groups and ANOVA for multiple groups, for the significance of difference and correlation between groups. Comparisons of statistical significance among multiple groups were determined using the Tukey's test when appropriate. A *p*-value of less than 0.05 was considered statistically significant.

3. Results

a) Characterization of EIS measurements in response to balloon inflation

The catheter-based balloon-inflatable concentric bipolar EIS was deployed into the phosphate saline buffer-filled explants of aorta in which EIS measurements were performed to determine the optimal inflation pressures (Fig. 3). At a balloon inflation pressure below 6 psi, the balloon was not fully inflated, and sensor was not in contact with the endoluminal surface. The EIS measurements revealed a baseline impedance magnitude of 70 kΩ at low frequency and more resistive behavior at a higher frequency, accompanied by −40 to −45 degrees of phase. At an inflation pressure of 7 psi, the inflated balloon enabled the microelectrodes to make contact with the vessel wall, resulting in a significant change in the impedance spectrum. At a low frequency, the magnitude of the impedance increased to 300 kΩ. At a high frequency, the magnitude of the impedance decreased as the vessel wall was more capacitive compared to that of saline, accompanied by a decrease in phase to −60 degrees at 100 kHz. At 9 psi, a slight decrease in magnitude and phase were observed, implicating a higher pressure applied by the balloon to the vessel wall causing local vessel wall deformation. Hence, our observations suggest that balloon inflation pressure at 7 psi allowed for both a complete surface contact and a minimum pressure to the arterial wall.

b) Ex vivo EIS measurements in fat-fed NZW rabbits

EIS measurements were performed in explants of fat-fed rabbit aorta via the balloon-inflatable concentric bipolar microelectrodes. Similar to the previous figure (Fig. 3), inflation of the balloon enables the sensor to be in contact with the endoluminal surface, and significant changes in both impedance magnitude and phase spectra were observed (Fig. 4a). Immunohistochemistry revealed lesion versus lesion-free sites in the insets, respectively (Fig. 4a and 4b). Balloon inflation-mediated endoluminal contact induced an approximately 20% increase in impedance magnitude from 1 kHz to 100 kHz, and a decrease in phase at a frequency above 50 kHz (n = 4). EIS sensor contact with the atherosclerotic lesions further resulted in a greater than 50% increase in the impedance magnitude spectrum over the entire frequency range (n =4), accompanied by a decrease in phase at the lower frequency range (1

kHz – 10 kHz), reflecting a more capacitive property of the tissue. Histological analysis confirmed the presence of foam cell-rich fatty deposition in the endoluminal vessel wall at the lesion sites in contrast to the lesion-free site with an intact tunica intima layer (inset in Fig. 4b). Hence, we demonstrate the feasibility of the balloon-inflatable concentric bipolar microelectrodes for intravascular interrogation.

c) In-vivo EIS measurements in NZW rabbits

We further demonstrated the deployment of the catheter-based balloon EIS sensor to interrogate carotid arteries of NZW rabbits (Fig. 6). The angiogram in Figure 5 revealed the position of the catheter in relation of the EIS sensor. The impedance of *in vivo* measurements displayed distinct phase spectrum compared to that of *ex vivo* findings (Fig. 4b) towards the lower frequency range. Both blood serum and vessel wall were more resistive as reflected in a higher phase changes at −34.1±1.6 and −30.4±0.3 degrees, respectively (n = 6). However, the impedance magnitude spectra in the frequency range of 10 kHz to 300 kHz displayed a similar pattern to that of Figure 4a. Balloon inflation induced an increase in impedance magnitude and a decrease in phase towards the higher frequency range. This observation is consistent with our previous findings that the EIS was most sensitive in detecting biological tissue compositions in the higher frequency range from 10 kHz to 300 kHz (Fei Yu et al., 2012).

4. Discussions

The novelty of the current study lies in the intravascular deployment of flexible and stretchable EIS technology to assess oxLDL-rich atherosclerotic lesions. Biological tissues harbor charges storing and dissipation properties, which can be measured by EIS (F. Yu, Ai, et al., 2011; Fei Yu et al., 2012). While the 4-point electrodes have been utilized, the linear arrays preclude the detection of small and non-homogenous lesions. Hence, our concentric bipolar microelectrodes provide a sensitive and reproducible strategy to detect electrochemical impedance at a close proximity to the lesions.

Despite the advent of computed tomographic (CT) angiography, high resolution magnetic resonance imaging (MRI) (Li et al., 2012), intravascular ultrasound (IVUS), near-infrared fluorescence (NIRF) (Jaffer et al., 2008) and time-resolved laser-induced fluorescence spectroscopy (Marcu, Fishbein, Maarek, & Grundfest, 2001), early identification of mechanically and metabolically unstable lesions remains an unmet clinical need. The features of flexible and stretchable electronics have made real-time endoluminal assessment of lipid-rich lesions possible. We have previously demonstrated flexible intravascular shear stress sensors (H. Yu et al., 2008). Here, we characterized the stretchable sensors in terms of distinct changes in impedance magnitude and phase spectra in response to various balloon inflation pressures (Fig. 4). We established baseline EIS measurements before and after balloon inflation, followed by comparing EIS magnitudes in the presence or absence of lipid-rich lesions. The inflation of the balloon at 7 psi enabled the EIS sensors to be in minimal contact area with the endoluminal surface, providing reproducible differences in both impedance magnitude and phase changes at frequencies above 30 kHz (Fig. 4 and 6). Furthermore, the EIS measurements supported our previously published reports in terms of elevated EIS in the oxLDL-rich regions (F. Yu, Ai, et al., 2011; Fei Yu et al., 2012). Thus,

we demonstrated the first intravascular sensor that is both flexible and stretchable for *in-vivo* applications.

Balloon inflation pressure at 7 psi is ideally suited for EIS measurements, and allows for both a complete surface contact and a minimum pressure to the arterial wall. While the difference in viscosity between saline and blood could affect the extent of balloon inflation, this difference is experimentally negligible. The bioengineering challenge resides in the higher intravascular blood pressure than atmosphere pressure or the pressure in saline, thus the balloon *in vivo* may not be inflated to the same extent as under the *in vitro* condition. In Fig. 3, we have demonstrated that EIS can detect lipid-rich lesions when in contact with the vessel wall. The impedance magnitude of blood is significantly lower than that of the vascular tissue due to its electrolyte-rich fluid property. For this reason, we can detect a significant increase in impedance magnitude when the inflated balloon makes contact between sensor and vascular wall. This phenomenon allows us to calibrate the extent of balloon inflation *in vivo*.

Oxidized low density lipoprotein (oxLDL) induces transformation of macrophages to lipid-laden foam cells (Brown & Goldstein, 1983). Activated macrophages secrete matrix metalloproteinase (MMPs) to mechanically destabilize plaques (Cheng et al., 1997; Y. S. Kim, Galis, Rachev, Han, & Vito, 2009). Growing evidence suggests that oxLDL and thin-cap fibroatheromas (TCFA) rich in macrophage/foam cells are prone to mechanical stress and destabilization (Chinetti-Gbaguidi et al., 2011; Ehara et al., 2001; Zeibig et al., 2011). Using our concentric bipolar microelectrode sensor, we demonstrated that oxLDL-laden foam cells in the subendothelial layer of plaque significantly increase the frequency-dependent EIS magnitude in New Zealand White (NZW) rabbits on diet-induced hyperlipidemia (F. Yu, Ai, et al., 2011). We further validated the electrochemical basis of EIS signals by assessing *in silico* electrical equivalent circuits at the electrode-endoluminal interface (F. Yu, Dai, Beebe, & Hsiai, 2011). Using explants of human coronary, carotid, and femoral arteries, we reproduced elevated EIS signals in the oxLDL-rich, but not oxLDL-free lesions (F. Yu, Dai, et al., 2011).

EIS measures the intrinsic electrochemical properties of the tissue; namely, water content, electrolyte concentration, vascular calcification and cholesterol/lipid content influence the frequency-dependent changes in impedance. Presence of active lipid or oxidized low density lipoprotein (oxLDL) in the endoluminal wall significantly reduces water content, which is electrically conductive. For this reason, an increase in frequency-dependent impedance magnitude in response to electrical input signals and an increase in capacitive effect in response to a high frequency range can be measured.

While EIS is a sensitive approach to assess lipid-rich lesions, its specificity would be strengthened by integrating with ultrasound (IVUS). While the high-frequency IVUS (20–60 MHz) will enable us to resolve spatial resolution from 400 μm to 30 μm, the concentric bipolar microelectrode sensor will detect distinct endoluminal impedance spectrum in the presence of high-fat versus normal diets (Streitner et al., 2009; Suselbeck et al., 2005). This integrated IUVS-EIS strategy will likely enhance the possibility of co-registration of ultrasound with the EIS measurements, and will detect an increase in EIS magnitude in non-

obstructive lesions that occupy less than 20% of the luminal diameter, but harbor oxLDL and foam cells (Fig. 4). Hence, integrating EIS with IVUS would improve both the sensitivity and specificity in identifying the metabolically active, but non-obstructive lesions (Suselbeck et al., 2005).

5. Conclusions

This current study presents the use of a robust and innovative balloon catheter-based concentric EIS sensor for the detection of endoluminal electrochemical properties. The demonstrations with explants from fat-fed NZW rabbit aortas and carotid arteries, respectively, further corroborated the link between endoluminal properties and lipid-rich lesions. The EIS strategy can further be integrated with intravascular ultrasound to strengthen and the sensitivity specificity in identifying unstable plaque.

Acknowledgments

The authors would like to express gratitude for technical advice from Dr. David Shavelle in the Division of Cardiovascular Medicine at USC, and technical support for animal studies from Sharon Hale and Dr. Robert Klonner in the Heart Institute at Good Samaritan Medical Center, Los Angeles. This project was supported by National Institutes of Health, HL083015 (T. K. H.) and HL111437 (T. K. H. and Y. C. T.).

References

Ai L, Rouhanizadeh M, Wu JC, Takabe W, Yu H, Alavi M, Hsiai TK. Shear stress influences spatial variations in vascular Mn-SOD expression: implication for LDL nitration. American Journal of Physiology- Cell Physiology. 2008; 294(6):C1576–1585. [PubMed: 18434620]

Ai L, Yu H, Dai W, Hale S, Kloner R, Hsiai TK. Real-time Intravascular Shear Stress in the Rabbit Abdominal Aorta. IEEE Transactions on Biomedical Engineering. 2009; 56(6):1755–1764. [PubMed: 19527952]

Aroom KR, Harting MT, Cox CS, Radharkrishnan RS, Smith C, Gill BS. Bioimpedance Analysis: A Guide to Simple Design and Implementation. Journal of Surgical Research. 2009; 153(1):23–30. [PubMed: 18805550]

Bamford J, Sandercock P, Dennis M, Burn J, Warlow C. Classification and natural history of clinically identifiable subtypes of cerebral infarction. Lancet. 1991; 337(8756):1521–1526. [PubMed: 1675378]

Brown MS, Goldstein JL. Lipoprotein metabolism in the macrophage: implications for cholesterol deposition in atherosclerosis. Annual Review of Biochemistry. 1983; 52(1):223–261.

Cheng GC, Briggs WH, Gerson DS, Libby P, Grodzinsky AJ, Gray ML, Lee RT. Mechanical strain tightly controls fibroblast growth factor-2 release from cultured human vascular smooth muscle cells. Circulation Research. 1997; 80(1):28–36. [PubMed: 8978319]

Chinetti-Gbaguidi G, Baron M, Bouhlel MA, Vanhoutte J, Copin C, Sebti Y, Tailleux A. Human Atherosclerotic Plaque Alternative Macrophages Display Low Cholesterol Handling but High Phagocytosis Because of Distinct Activities of the PPAR {gamma} and LXR {alpha} Pathways. Circulation Research. 2011; 108(8):985–995. [PubMed: 21350215]

Ehara S, Ueda M, Naruko T, Haze K, Itoh A, Otsuka M, Becker AE. Elevated levels of oxidized low density lipoprotein show a positive relationship with the severity of acute coronary syndromes. Circulation. 2001; 103(15):1955–1960. [PubMed: 11306523]

Foster KR, Schwan HP. Dielectric properties of tissues. Handbook of biological effects of electromagnetic fields. 1996:25–102.

Fung, YC. Biomechanics:Circulation. 2. Springer; 1997.

Hamilton RT, Asatryan L, Nilsen JT, Isas JM, Gallaher TK, Sawamura T, Hsiai TK. LDL protein nitration: Implication for LDL protein unfolding. Archives of Biochemistry and Biophysics. 2008; 479(1):1–14. [PubMed: 18713619]

Holvoet P, Mertens A, Verhamme P, Bogaerts K, Beyens G, Verhaeghe R, Van de Werf F. Circulating oxidized LDL is a useful marker for identifying patients with coronary artery disease. Arteriosclerosis, Thrombosis, and Vascular Biology. 2001; 21(5):844–848.

Holvoet P, Vanhaecke J, Janssens S, Van de Werf F, Collen D. Oxidized LDL and malondialdehyde-modified LDL in patients with acute coronary syndromes and stable coronary artery disease. Circulation. 1998; 98(15):1487–1494. [PubMed: 9769301]

Hsiai TK, Hwang J, Barr ML, Correa A, Hamilton R, Alavi M, Hazen SL. Hemodynamics influences vascular peroxynitrite formation: Implication for low-density lipoprotein apo-B-100 nitration. Free Radical Biology and Medicine. 2007; 42(4):519–529. [PubMed: 17275684]

Hwang J, Michael H, Salazar A, Lassegue B, Griendling K, Navab M, Hsiai TK. Pulsatile versus oscillatory shear stress regulates NADPH oxidase subunit expression: implication for native LDL oxidation. Circulation Research. 2003; 93(12):1225–1232. [PubMed: 14593003]

Hwang J, Saha A, Boo YC, Sorescu GP, McNally JS, Holland SM, Harrison DG. Oscillatory Shear Stress Stimulates Endothelial Production of O 2- from p 47 phox-dependent NAD (P) H Oxidases, Leading to Monocyte Adhesion. Journal of Biological Chemistry. 2003; 278(47):47291–47298. [PubMed: 12958309]

Jaffer FA, Vinegoni C, John MC, Aikawa E, Gold HK, Finn AV, Weissleder R. Real-time catheter molecular sensing of inflammation in proteolytically active atherosclerosis. Circulation. 2008; 118(18):1802–1809. [PubMed: 18852366]

Kim, Dae-Hyeong; Lu, Nanshu; Ma, Rui; Kim, Yun-Soung; Kim, Rak-Hwan; Wang, Shuodao; Islam, Ahmad. Epidermal electronics. Science. 2011; 333(6044):838–843. [PubMed: 21836009]

Kim YS, Galis ZS, Rachev A, Han HC, Vito RP. Matrix metalloproteinase-2 and-9 are associated with high stresses predicted using a nonlinear heterogeneous model of arteries. Journal of Biomechanical Engineering. 2009; 131(1):011009–011018. [PubMed: 19045925]

Konings MK, Mali Wptm, Viergever MA. Development of an intravascular impedance catheter for detection of fatty lesions in arteries. IEEE transactions on medical imaging. 1997; 16(4):439–446. [PubMed: 9263001]

Li, Rongsong; Mittelstein, David; Lee, Juhyun; Fang, Karen; Majumdar, Rohit; Tintut, Yin; Hsiai, Tzung K. A dynamic model of calcific nodule destabilization in response to monocyte-and oxidized lipid-induced matrix metalloproteinases. American Journal of Physiology-Cell Physiology. 2012; 302(4):C658–C665. [PubMed: 22031601]

Marcu L, Fishbein MC, Maarek JMI, Grundfest WS. Discrimination of human coronary artery atherosclerotic lipid-rich lesions by time-resolved laser-induced fluorescence spectroscopy. Arteriosclerosis, Thrombosis, and Vascular Biology. 2001; 21(7):1244–1250.

Streitner I, Goldhofer M, Cho S, Thielecke H, Kinscherf R, Streitner F, Suselbeck T. Electric impedance spectroscopy of human atherosclerotic lesions. Atherosclerosis. 2009; 206(2):464–468. [PubMed: 19419719]

Suselbeck T, Thielecke H, Kochlin J, Cho S, Weinschenk I, Metz J, Haase KK. Intravascular electric impedance spectroscopy of atherosclerotic lesions using a new impedance catheter system. Basic Research in Cardiology. 2005; 100(5):446–452. [PubMed: 15795794]

Verhamme P, Quarck R, Hao H, Knaapen M, Dymarkowski S, Bernar H, Gabbiani G. Dietary cholesterol withdrawal reduces vascular inflammation and induces coronary plaque stabilization in miniature pigs. Cardiovascular Research. 2002; 56(1):135–144. [PubMed: 12237174]

Virmani R, Kolodgie FD, Burke AP, Farb A, Schwartz SM. Lessons from sudden coronary death: a comprehensive morphological classification scheme for atherosclerotic lesions. Arteriosclerosis, Thrombosis, and Vascular Biology. 2000; 20(5):1262–1275.

Yu F, Ai L, Dai W, Yu H, Hsiai TK. MEMS Thermal Sensors to Detect Changes in Heat Transfer in the Pre-Atherosclerotic Regions of Fat-Fed New Zealand White Rabbits. Annals of Biomedical Engineering. 2011; 39(6):1736–1744. [PubMed: 21380571]

Yu F, Dai X, Beebe T, Hsiai T. Electrochemical impedance spectroscopy to characterize inflammatory atherosclerotic plaques. Biosensors and Bioelectronics. 2011; 30(1):165–173. [PubMed: 21959227]

Yu, Fei; Lee, Juhyun; Jen, Nelson; Li, Xiang; Zhang, Qian; Tang, Rui; Hsiai, Tzung K. Elevated electrochemical impedance in the endoluminal regions with high shear stress: Implication for assessing lipid-rich atherosclerotic lesions. Biosensors and Bioelectronics. 2012

Yu, Hongyu; Ai, Lisong; Rouhanizadeh, Mahsa; Patel, Darhsin; Kim, Eun Sok; Hsiai, Tzung K. Flexible polymer sensors for in vivo intravascular shear stress analysis. Journal of microelectromechanical systems. 2008; 17(5):1178–1186.

Zeibig S, Li Z, Wagner S, Holthoff HP, Ungerer M, Bultmann A, Gawaz M. Effect of the oxLDL Binding Protein Fc-CD68 on Plaque Extension and Vulnerability in Atherosclerosis. Circulation research. 2011; 108:695–703. [PubMed: 21293004]

1. Our concentric bipolar microelectrodes enabled highly sensitive EIS measurement of the electrochemical tissue properties at close proximity without interference from the surroundings.
2. Balloon inflation allowed EIS sensors to be in contact with endoluminal surface. The EIS sensors remain functional under inflation condition due to the smart design.
3. Our findings demonstrated the potential clinical utility of stretchable EIS sensors to identify lipid-rich atherosclerotic lesions with an implication for unstable plaques.

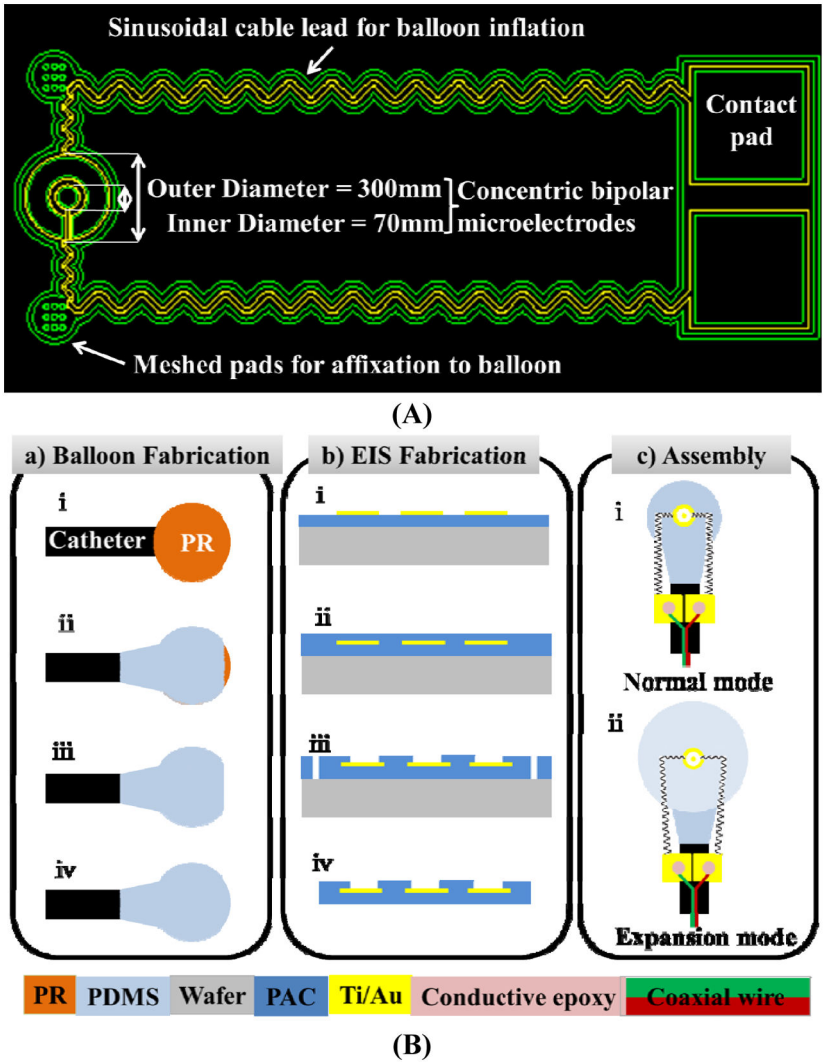

Fig. 1.

(A) The concentric bipolar microelectrodes. The impedance sensor on the left was designed to mount on the surface of the balloon and the contact pads on the right were to affix onto the catheter. The two sinusoidal leads connecting between the contact pads and the impedance sensor were allowed to be stretched in both x- and y-direction in response to balloon inflation. The meshed gluing pads were patterned with 9 opening holes to facilitate affixation to the balloon via the biocompatible glue. **(B)** Microfabrication of balloon inflatable concentric bipolar microelectrodes. (a) Balloon fabrication: (i) A droplet of photoresist (PR) formed on the tip of a catheter tube. (ii) Silicone partially coated the PR droplet while allowing the tip to be opened. (iii) PR was removed. (iv) The tip was sealed with silicone, resulting in a balloon. (b) Fabrication of the concentric bipolar microelectrode sensor: (i) Standard parylene C (PAC) was deposited and metal was patterned for both the sensor and electrode leads. (ii) A 2nd PAC coating sealed the metal. (iii) At the terminal end of the sensor and the contact pads, lithography was performed, followed by O_2 plasma etching of PAC to open the sensor electrodes and the contact pads, and to define the edges of the sensor and the leads. (iv) After lift-off from the substrate, the terminal end of the

sensor was completely free-standing. Assembly of the balloon and sensor: (i) The impedance sensor was mounted on the non-inflated balloon by the two meshed gluing pads. The two contact pads were affixed onto the catheter tube. (ii) The inflated balloon stretched the sensor cables in both x- and y-direction.

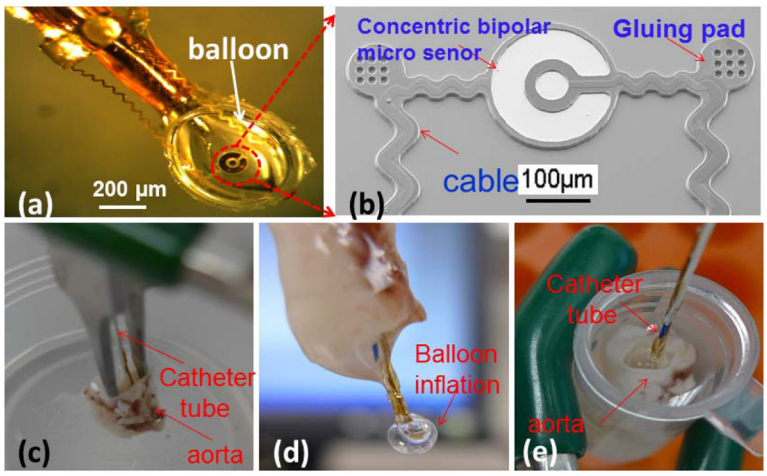

Fig. 2.

Characterization of balloon-inflatable concentric bipolar microelectrode sensor. (a) The impedance sensor was mounted on a balloon. (b) SEM photo of the finished impedance sensor, highlighting the stretchable sinusoidal cables in response to balloon inflation and the two gluing pads allowed for affixation on the surface of the balloon. (c) The balloon impedance sensor was inserted into the *ex-vivo* rabbit aorta. (d) Demonstration of balloon inflation prior to impedance assessment. (e) Demonstration of intravascular balloon inflation.

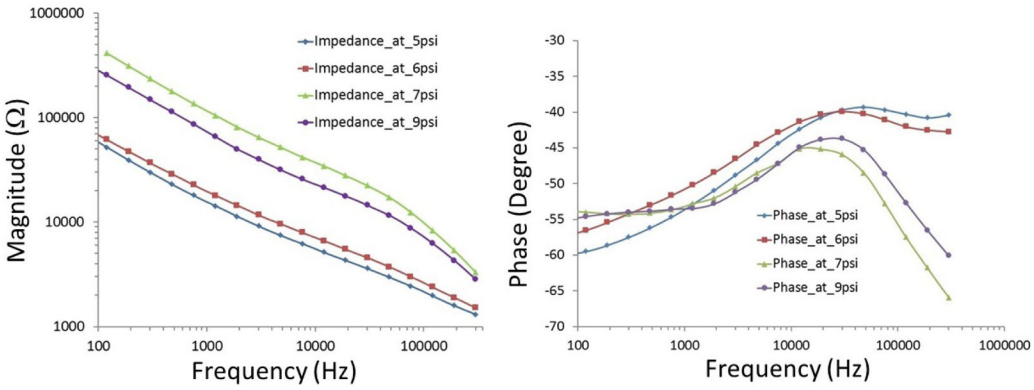

Fig. 3.

Characterization of balloon-inflatable impedance sensor in terms of frequency-dependent changes in impedance magnitude and phase. Data were collected in response to balloon inflation at 5, 6, 7 and 9 psi, respectively. The data revealed that 7 psi was sufficient for adequate contact between the sensor and vessel wall as it showed a significant change in the values at the whole frequency band with magnitude and at frequencies above 30 kHz with phase. At 9 psi, the balloon was over-inflated representing a slight decrease.

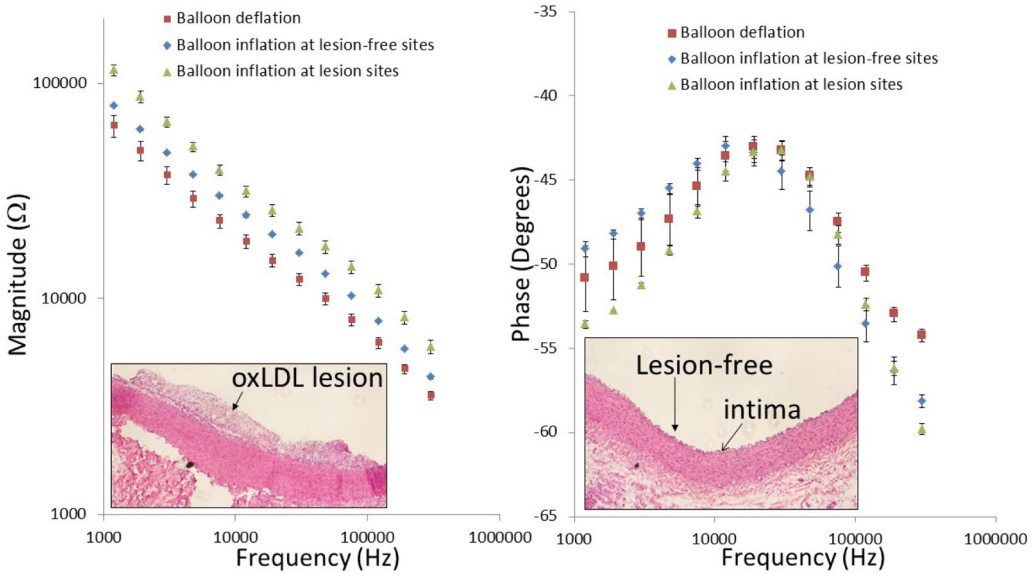

Fig. 4.

Ex-vivo EIS acquisition from explanted rabbit aorta and corresponding histology of the aorta wall. After 8 weeks of high-fat diet, rabbits were sacrificed and aortas were extracted and fixed in 15% paraformal aldehyde (PFA). The individual aortas were sectioned into 2–3cm segments and immersed in PBS for deployment of the balloon-inflatable EIS sensor. Endoluminal lipid deposition or atherosclerotic lesions were visible for EIS interrogation and comparison with the disease-free sites. (a) After the balloon inflation, the impedance magnitude increased over the entire frequency range from 1 kHz to 1,000 kHz. EIS measurement further increased significantly at the lesion sites. (b) Corresponding histology revealed intact tunica intima and media layer at lesion-free sites, and accumulation of foam cells at lesion sites.

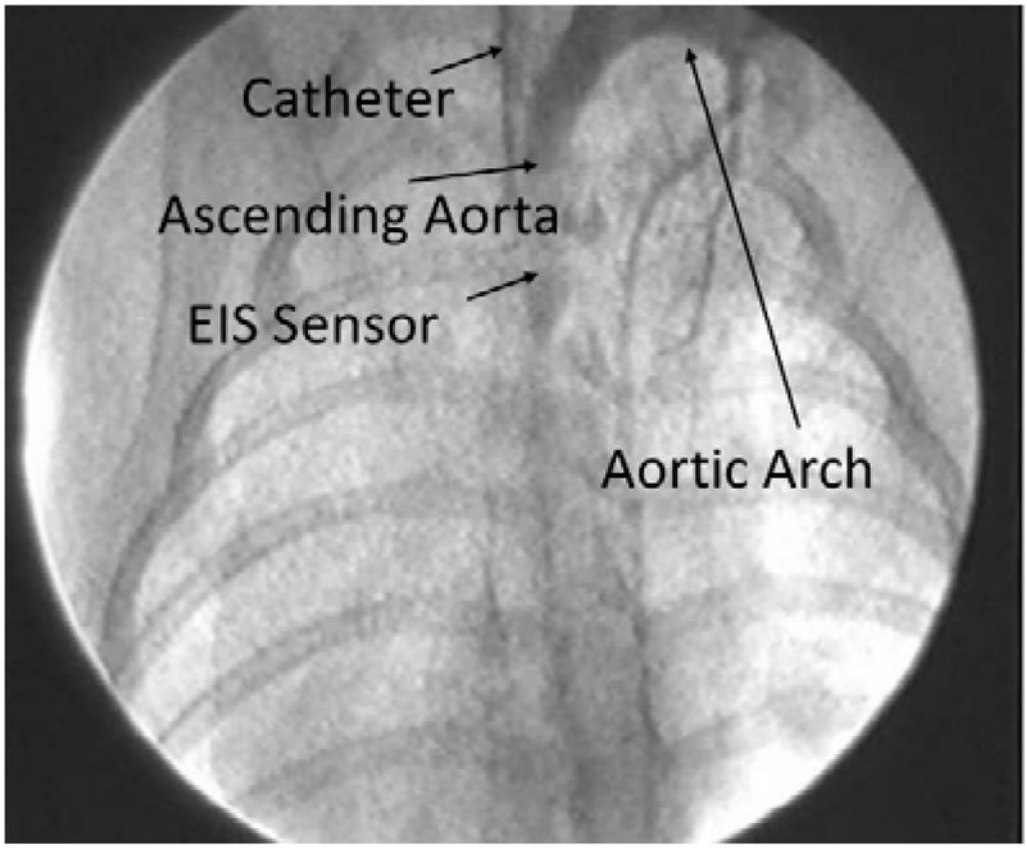

Fig. 5.
Deployment of balloon-inflatable EIS sensors via fluoroscopy guidance in NZW rabbits. The position of EIS sensor was visualized in the carotid artery.

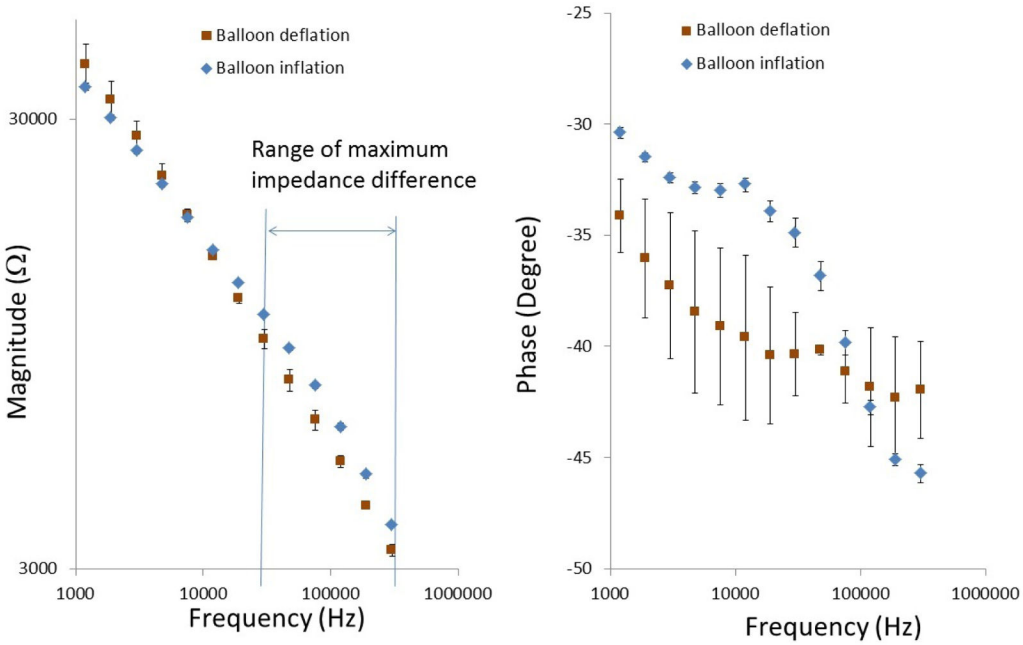

Fig. 6.

In-vivo EIS acquisition in the rabbit carotid arteries. Balloon-inflatable EIS sensor packaged onto an in-house built balloon catheter. Catheter was deployed through right carotid artery cut-down and the sensor was made endoluminal contact under the fluoroscopic guidance. Inflation of balloon resulted in a significant increase in the frequency-dependent impedance magnitude from 10 kHz to 300kHz, along with the distinct phase characteristics.